NRIAG Journal of Astronomy and Geophysics (2015) **4**, 86–99

National Research Institute of Astronomy and Geophysics

NRIAG Journal of Astronomy and Geophysics

www.elsevier.com/locate/nrjag

Integration of geophysical and geological data for delimitation of mineralized zones in Um Naggat area, Central Eastern Desert, Egypt

Ibrahim Gaafar

Nuclear Materials Authority, Egypt

Received 28 January 2015; revised 22 April 2015; accepted 28 April 2015
Available online 30 May 2015

KEYWORDS

Airborne magnetic;
Gamma-ray spectrometric;
Rare metal mineralization

Abstract An integrated approach for geophysical, geological and mineralogical data was followed for Um Naggat area, Central Eastern Desert, Egypt, in order to delineate its mineralized zones. The albitized granites are well-defined on the Th- and U-channel images, by their anomalous shapes, reaching 150 ppm and 90 ppm respectively, beside low K content.

Interpretations of the aeromagnetic maps delineated four regional structural trends oriented due NNW, NW, ENE and E–W directions. They are identified as strike-slip faults, which coincide well with field observations, where NW-trending faults cut and displace right laterally ENE-trending older ones. The interaction between these two strike-slip fault systems confining the albite granite is easily identified on the regional data presenting longer wavelength anomalies, implying deep-seated structures. They could represent potential pathways for migration of enriched mineralized fluids. Geochemically, albite granites of peraluminous characteristics that had suffered extensive post-magmatic metasomatic reworking, resulted into development of (Zr, Hf, Nb, Ta, U, Th, Sn) and albite-enriched and greisenized granite body of about 600 m thick, and more than 3 km in strike length. The albite granite is characterized by sharp increase in average rare metal content: Zr (830 ppm), Hf (51 ppm), Nb (340 ppm), Ta (44 ppm), and U (90 ppm). Thorite, uranothorite, uraninite and zircon are the main uranium-bearing minerals of magmatic origin within the enclosing granite. However, with respect to Zr, Nb, and Ta, the albitized granite can be categorized as rare metal granite. The integration of airborne geophysical (magnetic and γ-ray spectrometric), geological, geochemical and mineralogical data succeeded in assigning the albite granite of Um Naggat pluton as a mineralized zone. This zone is characterized by its high thorium and uranium of

E-mail address: Ibrahim.gaafar@hotmail.com

Peer review under responsibility of National Research Institute of Astronomy and Geophysics.

Production and hosting by Elsevier

http://dx.doi.org/10.1016/j.nrjag.2015.04.004

hydrothermal origin as indicated by its low Th/U ratio, with rare metals mineralization controlled by two main structural trends in the NW- and ENE-directions.

1. Introduction

Several studies have shown the advantages, disadvantages, benefits and limitations of uses of geophysical methods in detailing and analysing the morphology of mineral deposits (Irvine and Smith, 1990; White et al., 2001; Moreira and Ilha, 2011; Moreira et al., 2012). The most commonly used first step in a geophysical exploration process is aeromagnetic survey, permitting detection of ambient magnetic fields caused by magnetic minerals that are present in the ground. Magnetic maps are often used in conjunction with other geophysical survey methods such as radiometrics, and VLF-EM to create more comprehensive geophysical and geological picture of the survey area (Gaafar, 2012). Airborne magnetic and radiometric surveys were used extensively in mineral exploration industry, predominantly for the delineation of metalliferous deposits (Airo and Loukola-Ruskeeniemi, 2004). Its application ranges from mineral exploration (Murphy, 2007), structure mapping and rock characterization (Telford et al., 1990). Recent advances in technology have substantially increased the accuracy and resolution of these techniques so that they can be used to provide useful enhanced information on lithology and structure. The increasing use of gamma-ray spectrometry over the past decades indicates that it will play a more important role in geological mapping and mineral exploration in the future.

Effective integration leads directly to increased success potential and reduced exploration risk. Analysis of geophysical features provides new insights into structural framework and can help geologists to target new areas for mineral exploration. The interpretation of high-resolution magnetics has provided an overview of the regional structure as well as further insight into structural controls of the albite-hosted-rare metal mineralization.

Integrated geophysical exploration programmes proved to be successful in identifying the sub-surface evidences of mineralization or associated structures/alteration zones (e.g., Mohanty et al., 2011; Chaturvedi et al., 2013; Patra et al., 2013; Gaafar, 2014). However, detailed geophysical studies have never been carried out for delineation of alteration zones and rock types associated with uranium and rare-metal mineralization of the region. Therefore, in the present study, an integrated geophysical investigation using magnetic, spectrometric and geochemical data was carried out in and around the mineralization zones of Um Naggat area. Various anomalous zones were compared with each other and geologic maps to evaluate their effectiveness for displaying uranium and rare-metal mineralization and know their geophysical signatures.

2. Geologic outlines

Um Naggat area is situated in the Central Eastern Desert of Egypt at the watershed of Wadi Um Gheig draining to the Red Sea and Wadi E1-Miyah draining to the Nile basin, between Latitudes 25°28 and 25°31′N and Longitudes 34°09 and 34°18E (Fig. 1).

The lithostratigraphic rock units cropping out in Um Naggat area comprise metavolcanics, meta-gabbros, granodiorites, biotite granites and albite granites (Fig. 1). Metavolcanics are characterized by moderate to high relief, with deep brown colour. They are found in several localities in the northern parts of the studied area (Fig. 1, modified after Greiling et al., 1988). The grain size is fine. There is a sharp contact between metavolcanics and both biotite and albite granites. The metavolcanic rocks were interpreted as old metavolcanics of low-K tholeiitic basalts, which were an integral part of an ophiolite association and young metavolcanics which belong to the island arc association of andesite and volcanic lastics (Stern, 1981; El-Gaby et al., 1988). Metavolcanics of the study area belong to island arc metavolcanics. Metagabbros have different grain sizes that range from coarse-grained to pegmatitic ones, with dark green to grey colour. They are found in the south western part of the studied area with clear contacts with younger granites. The interaction of these metagabbros with the invading granite material changed them towards diorites, giving metagabbro-diorite complex. Older granites are the oldest intrusive granitic rocks in the studied area and characterized by moderate to low relief hills of medium to coarse-grain size. They are found at the southeastern part of the studied area, and have xenoliths from the previous rock types. They have grey to pale grey colour, according to the amount of mafic minerals. The composition of older granites ranges from tonalite to granodiorite.

Um Naggat granitic body comprises two granitic types, the biotite granite and alkali feldspar granite. The biotite granite is mainly composed of quartz, K-feldspar, plagioclase and biotite. Zircon, apatite, allanite, sphene and iron oxides are the main accessories. The alkali feldspar granite is mainly composed of alkali feldspar, plagioclase, quartz, biotite and muscovite. Zircon, allanite and opaque minerals are the main accessories. The episyenites are recorded as a result of quartz leaching out with red colour of the whole rock due to the presence of K-feldspars or hematization in some places, along the NW–SE and N–S fault planes. It must be noticed that the wide area in the eastern part of the Um Naggat granitic pluton is covered by Wadi sediments and represented by some small episyenitized parts at its boundary, which can be taken as evidence for the possible presence of larger episyenitization at deeper parts. Trachyte plugs are found in the studied area in its southern part and have a sharp contact with biotite granite. These plugs are massive or blocks and may be found as cone-shaped one. Trachyte has a grain size that ranges from fine to medium. Besides, it has a porphyritic texture with alkali feldspar phenocrysts, and fragments of biotite granite.

The contacts of the granite dip steeply towards the country rocks. On the northern side, the form of the granite is complicated by several dome shaped projections up to 1 km in diameter which created favourable structures for intensive

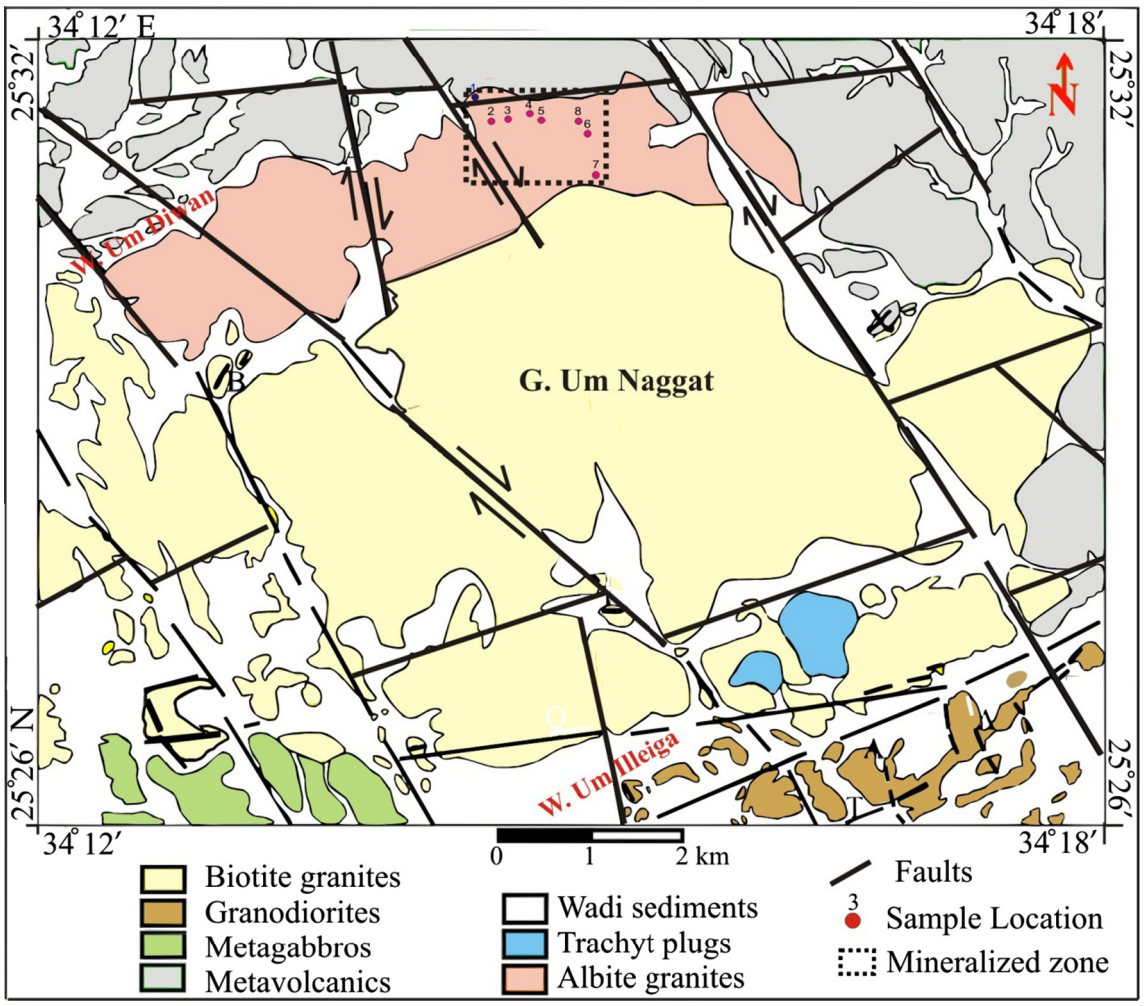

Fig. 1 Geologic map of Um Naggat area, Central Eastern Desert, Egypt (modified after Greiling et al., 1988).

metasomatic alteration of the original granite and the formation of ore mineralization. The presence of small outcrops of altered granite among the country rocks of the northern contact of the massif indicates the existence of favourable conditions for ore formation in dome-shaped structures, unaffected by erosion. Among the granite a series of facies are distinguished, representing metasomatically altered rocks. The granite facies are successively replaced by one another from the northern contact deep into the massif. The central and the southern parts of the massif are mainly composed of unaltered coarse-grained amphibole granite which may be considered as the original parent granite (Sabet et al., 1976).

The albite granite forms an oval-shaped body of about 0.6 km × 3 km. It is characterized by a huge mass that possesses the highest relief in the studied area (1300 m above sea level), with irregular boundaries in its eastern side and flatness in the E–W direction. It is composed mainly of medium- to coarse-grained biotite granite and enveloped by albite granite from the northern part. Pegmatite bodies of lensoid shape, up to 3.0 m long and 1.0 m wide, are located along the northern marginal zone of the albitized granite. The albitized granite is represented by a highly altered zone, which ranges from 50 m to 250 m in width and up to 7 km in length. There are much alteration processes as albitization, greisenization, kaolinization and fluoritization associated with the albitized granite, especially along major sinistral faults striking in a NW–SE direction. Albitization is a process of a base exchange between interacting, high temperature, alkaline fluids and early formed feldspars within nearly consolidated granite, thus, resulting into enrichment of the rock in albite. Many quartz veins were invaded in this zone. Um Naggat granite has sharp contacts and is intruded into older granites from the south; and metagabbro and metavolcanics from northern, eastern and western parts. Um Naggat body was affected by many faults and invaded by trachyte dikes and plugs especially in the NW–SE and N–S trends. Contacts with the country rocks are irregular, sharp and of an intrusive nature. Pegmatitic and appinitic gabbro patches are locally present, particularly along contacts with granites.

3. Methodology

Airborne magnetic and gamma-ray spectrometric data were acquired, in 1984, by Aero-Service, over the Eastern Desert of Egypt including the study area. The survey was flown using fixed-wing aircraft equipped with a high-sensitivity system. The survey was carried out along a set of parallel flight lines

Table 1 Major elements, trace elements and REE compositions of the Um Naggat area.

	Nag1	Nag2	Nag3	Nag4	Nag5	Nag6	Nag7	Nag8
SiO_2 (%)	**83.7**	**77.7**	**78**	75	**78.5**	**77.5**	76.5	***66.1***
Al_2O_3 (%)	9.8	12.3	11.7	13.4	11.4	11.9	11.8	**18.2**
Fe_2O_3 (%)	0.6	**1.2**	**1.4**	**1.4**	**1.2**	**1.3**	**1.5**	0.6
MgO (%)	0.1	0	0	0	0.1	0.1	L.D.	0.1
CaO (%)	2.1	0.1	0.1	0.1	0.1	0.2	0.2	0.1
Na_2O (%)	***0.2***	3.9	3.9	5	3.6	4	4.3	**5.3**
K_2O (%)	***1.8***	4.1	4	4.3	4.2	4.1	4	**8.1**
IL (%)	**2.6**	0.9	0.8	0.7	0.7	0.7	0.6	0.6
Total (%)	100	100	100	100	100	100	99	99
As (ppm)	**21**	1.8	L.D.	L.D.	L.D.	2	L.D.	L.D.
Ba (ppm)	**52.1**	14.3	13.3	6.1	14.7	30.2	13.3	22
Be (ppm)	4.2	5.4	7.5	5.7	5.4	3.2	2.6	4
Bi (ppm)	9.4	1.9	1	1.1	0.9	0.5	4.2	0.2
Cd (ppm)	1.1	0.5	1.3	0.3	0.7	0.8	1	0.2
Ce (ppm)	17.1	57.1	58	55	22.2	**150**	**138**	**114**
Cr (ppm)	30.2	15.4	20	22.2	13.5	24.5	**39**	15
Cs (ppm)	4.6	3.8	5.8	4.7	5.4	1.5	1.4	2.3
Cu (ppm)	13.4	L.D.	L.D.	L.D.	L.D.	23.6	8.6	L.D.
Dy (ppm)	13	13	16	6.7	8	**15**	**12**	**18**
Er (ppm)	18	17	**25**	6.9	14	10	9.1	**19**
Eu (ppm)	0.1	0.1	0.1	0	0	0.2	0.1	0
Ga (ppm)	39	54	53	60	52	48	46	67
Sm (ppm)	2.3	3.9	5.7	4.8	1.3	15	8.8	8
Sn (ppm)	**83**	23.8	38.1	**52.7**	**55.3**	**65.1**	**96.4**	3.6
Sr (ppm)	30	13	8.8	6.6	6.6	6.8	9.8	10
Ta (ppm)	113	46.2	59	29	51	18.5	12.7	19.4
Tb (ppm)	1.2	1.2	1.5	0.9	0.7	2.5	1.8	2.2
Th (ppm)	**166**	**67**	**69**	46	**63**	30.3	19.5	22.9
Tm (ppm)	5	4.5	7	1.9	4.2	2.2	1.8	4.4
U (ppm)	**62**	**49**	**50**	**23**	**65**	**10**	9	7.3
W (ppm)	8.3	3.8	5	2.7	4.8	2.5	1.6	1.9
Y (ppm)	**117**	75	**99**	35	43	94	**129**	**181**
Yb (ppm)	**49**	**42**	**69**	20	**44**	19	15.2	**39**
Zn (ppm)	41.6	**405**	**245**	**277**	**216**	**534**	**419**	77.2
Zr (ppm)	**1391**	**740**	**2022**	**404**	**1196**	**350**	**224**	**297**
Gd (ppm)	3	3.5	4.5	3.6	1.4	11.7	8.2	7.6
Ge (ppm)	2.9	3.7	**4.5**	4.3	3.9	3.1	2.9	4.3
Hf (ppm)	**102**	**49**	**109**	28.5	**72**	20.3	14.9	22.5
Ho (ppm)	3.8	3.6	4.9	1.5	2.5	3	2.7	4.6
In (ppm)	0.7	0.3	0.4	0.3	0.3	0.6	0.4	L.D.
La (ppm)	5.5	24.4	34.4	27.2	8	**129**	**78**	**60**
Lu (ppm)	8.9	7.4	12.5	3.5	8	3.1	2.5	6.1
Mo (ppm)	**190**	4.5	4.3	1	3.3	2	1.7	1.7
Nb (ppm)	**672**	**439**	**536**	**201**	**485**	**172**	**104**	**120**
Nd (ppm)	5.3	15.9	23.4	17.7	5	**67**	**39**	**33**
Pb (ppm)	434.1	9.4	10.6	17.3	15.8	10.5	10.8	17.2
Pr (ppm)	1.6	6	8.9	6.6	2	25	14	11.3
Rb (ppm)	**369**	**631**	**781**	**778**	**746**	**439**	**307**	**1021**
Si	1394	1294	1300	1250	1308	1291	1274	1102
Al	192	242	229	262	224	233	231	358
Fe	6.9	14.4	17.3	17.4	14.5	15.7	18.9	7.4
Mn	0.6	0.3	0.5	0.5	0.5	0.8	0.9	0.5
Ca	36.5	2.4	2.4	1.7	1.7	2.9	4.1	2.2
Na	6.5	125	126	160	116	130	138	170
K	37.7	86.4	84.6	91.1	90.1	87.2	85.4	173
K metal	1.5	3.4	3.3	3.6	3.5	3.4	3.3	6.7
Ti	0	0.4	0.4	0.3	0.4	0.6	0.7	0
P	−5	−41	−44	−71	−27	−46	−56	0
Q	**396**	**218**	**221**	164	**229**	**211**	**199**	22
B	7	15	18	18	15	16	20	7
A	75	25	13	7	14	10	0	10

Bold-italic values represent the low values than normal. Bold values represent the high values than normal.

maintaining 1.0 km line spacing and NE–SW direction. Nominal sampling interval and flight height were 90 m and 120 m terrain clearance, respectively (Aero-Service, 1984).

Geophysical processing consisted of verifying and gridding magnetic and spectrometric airborne survey data using a variety of software. The major software used to process and enhance the data is the Geosoft (Oasis Montaj). Other geophysical softwares were used to enhance the data in a variety of formats such as Golden Software Surfer 10 and Grapher 7.

During detailed field observations, eight samples were collected for geochemical analyses throughout three rock types: the albitized granite, pegmatite and episyenite, cropping out in the geophysically determined mineralized zone of Um Naggat area. After agate mortar crushing, the rocks were analysed by ICP-AES and ICP-MS (SARM, CRPG, Nancy, France) for 11 major and 44 trace elements (Table 1).

4. Results

4.1. Airborne γ-ray spectrometric data

Airborne gamma-ray spectrometric data are often used as a powerful tool to aid both mineral exploration and geological (lithological and structural) mapping. Um Naggat area is an excellent example for illustrating the usefulness of gamma-ray spectrometric data to support modern geological mapping and mineral exploration in arid terrains. Analyses of K, Th and U channel images, displayed as composite themes, correlate well with main regional framework of Um Naggat area. Several distinct mapped radiometric–lithologic units are easily distinguishable in the gamma-ray spectrometric data. Definition of the contacts among units, faults and shapes of granitic intrusions is considerably enhanced by the airborne gamma ray spectrometric data. The results here presented show that there is a strong relationship among geochemical, mineralogical and geophysical signatures of different rocks in the studied area.

Despite the fact that aeromagnetic data are still the best way to discriminate structural features, gamma-ray spectrometry turned out to be also an excellent tool to distinguish different superposed structural events overprinted in the rocks, at least as far as their surface signatures are concerned. Thus, the spectrometric data are able to identify regional and more detailed scale structures as shown on the three radioactive maps (Figs. 2–5), which makes possible the individualization of different structural domain boundaries that coincide with abrupt changes in radiometric trends. Geometry and contacts of granite bodies and faults are characterized by abrupt contrasts between high- and low-intensity anomalies in narrow and straight linear belts, parallel to the regional trend. A predominant NW-trend of the structures in the studied area is evident, mainly in the Th-channel data and in the ternary image data (Figs. 3 and 5). Another important feature is the faulting of the ENE trending structures. The youngest NW trending structures of dextral sense movement are continuous and cross the oldest, ENE-trending structures, then displacing.

The albitized granites are well-defined on the Th- and U-channel images, by their anomalous shapes, reaching 150 ppm and 90 ppm respectively (Figs. 2 and 3). Potassium radiation essentially comes from K feldspar, predominantly microcline and orthoclase or micas such as muscovite and biotite which are common in felsic igneous rocks (e.g., granite) and are low in mafic rocks (e.g., basalt and andesite), but virtually absent from dunite and peridotites (Manu, 1993). Comparing K-map (Fig. 2) with the geologic map (Fig. 1), the elongated high K concentrations are linearly distributed in the NE- and NW-directions, representing the coarse-grained biotite granite. The albite granites have moderate K

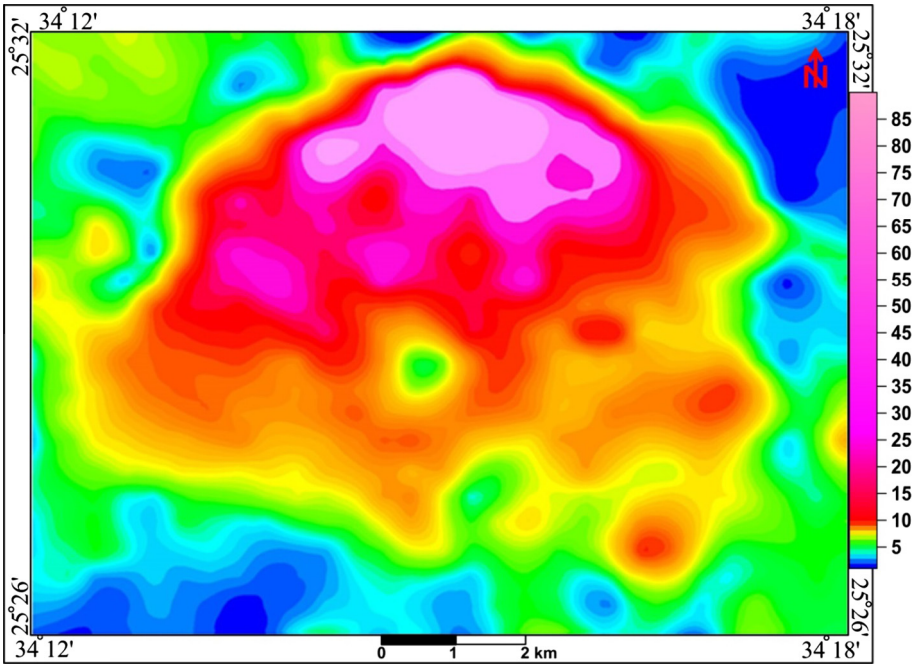

Fig. 2 Airborne eU (ppm) image map of Um Naggat area, Central Eastern Desert, Egypt.

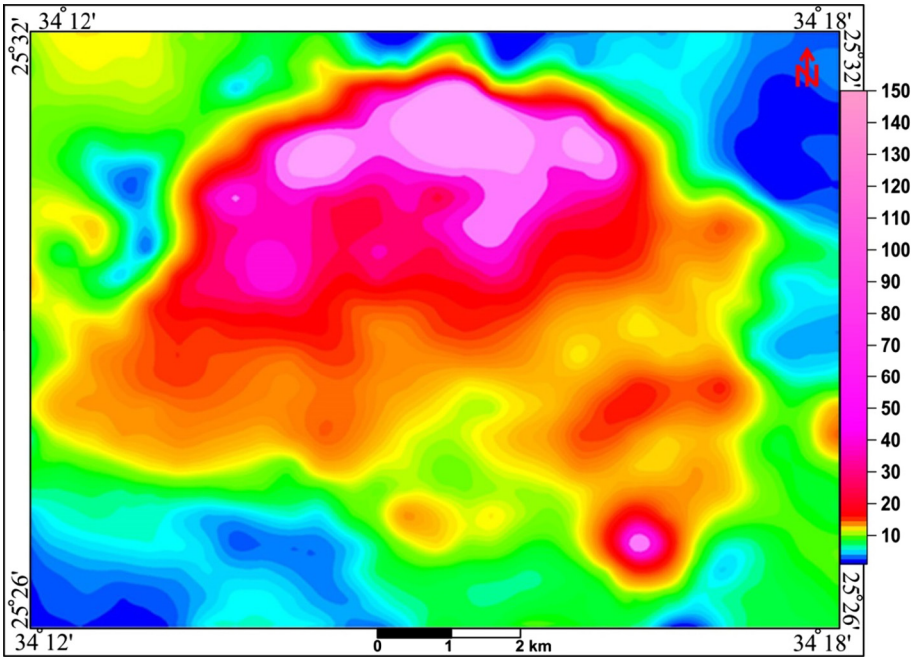

Fig. 3 Airborne eTh (ppm) image map of Um Naggat area, Central Eastern Desert, Egypt.

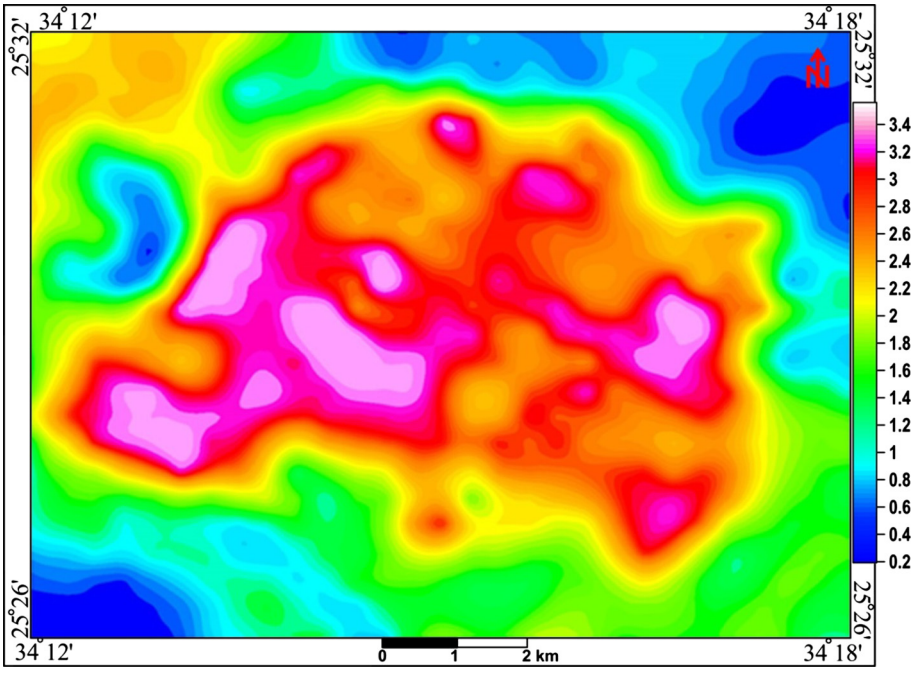

Fig. 4 Airborne K (%) image map of Um Naggat area, Central Eastern Desert, Egypt.

concentrations, but metavolcanics and metagabbros have low K concentrations. Generally, high Th concentrations are related to felsic minerals and low Th concentrations are related to mafic minerals (Shives, 2008). The strong thorium concentration in Um Naggat area is a result of the presence of albite granite. Thorium is generally considered very immobile (Silva et al., 2003); thus, the regions with high thorium concentration suggest that Th was mobilized in hydrothermally-altered systems. The low Th patterns represent alteration patterns in the different rocks and along lithologic boundaries. Among these regions are, also, faults and shears (Fig. 3) hosting hydrothermal fluids, which leach Th. Unlike, K map, U map (Fig. 4) clearly indicates distinct boundary between albite granite of high U-concentration and biotite granite of intermediate

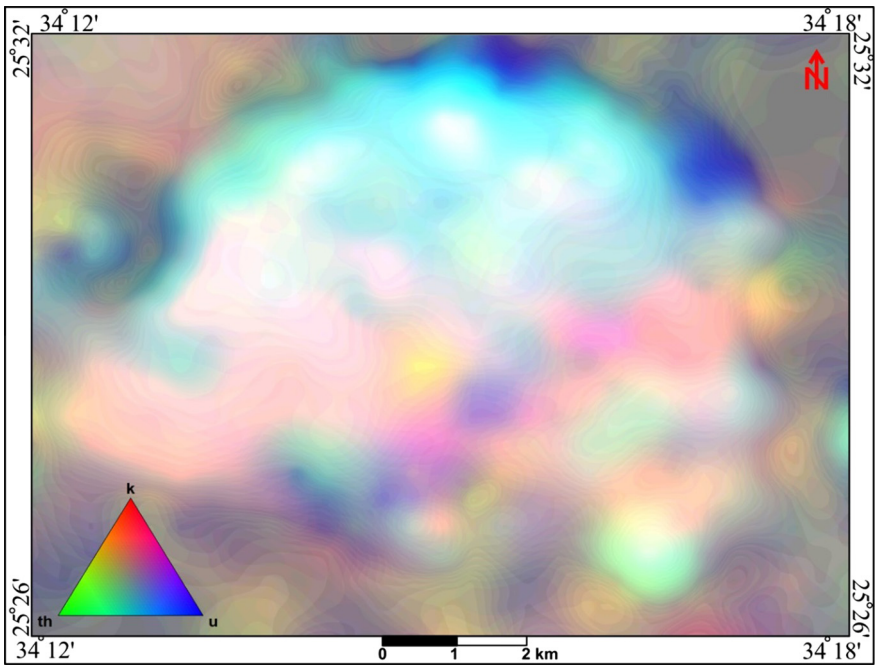

Fig. 5 Airborne ternary composite image map of Um Naggat area, Central Eastern Desert, Egypt.

level, that agree well with Th-map. The high U and Th-concentrations are associated with albite granite, beside low K content.

The three spectrometric maps were individually enhanced and then displayed in a pseudo-colour composition (R:B:G = K:eU:eTh). There is an obvious relationship between some mapped geologic units and the spectrometric data.

Individual lithological units can be traced due to their distinctive spectrometric signatures. The Ternary image (Fig. 5) comprises various colours generated from the relative intensities of the three components and represents subtle variations in the ratios of the three bands. Potassium was assigned to red, uranium to blue and thorium to green. The metavolcanics and metagabbro appear darker than the surrounding units, indicating lower concentrations in K, U and Th. The white areas in the ternary image are indication of high concentrations of the three radioelements, potassium, thorium and uranium, resulting from the existence of albitized granite. The magenta shows areas of high K and U, but low Th concentrations, while the yellow indicates areas of high K and Th but low U concentrations. The ternary map shows high U and Th concentrations related to albitized granite. Besides, high Th and U contents of these granites agree well with enriched Nb, Ta, Zr, and Hf parts of this granite.

4.2. Airborne magnetic data

Aeromagnetic data are commonly used for regional-scale geological mapping and in the search for mineral deposits directly associated with magnetic minerals. Magnetic anomalies in the earth's magnetic field are caused by magnetic minerals in the rocks, and maps of these anomalies can be interpreted in terms of geology (Silva et al., 2003). The main goal for use of magnetic data is to delineate lithology and structure, which normally serve as conduits for hydrothermal fluid deposition. On a regional scale, airborne geophysical data have often been used to identify several features, such as limits of geologic provinces, fold belts, sedimentary basins and tectonic and structural details of shear zones and overprinted structural trends (Schetselaar, 2001; Direen et al., 2001). Geological concepts are applied for targeting structural settings favourable for rare-metal deposits, using detailed magnetic images. They are also used to locate subsurface prospective of typical outcrops. It is the identification of these favourable structural settings, which has led to the increased use of aeromagnetic data in rare metal deposit exploration.

The map of RTP magnetic data (Fig. 6) shows the observed magnetic anomalies directly over the magnetic source bodies and sharpens the contacts between the magnetic high and low patterns as well as anomalously high magnetic susceptible zones probably coming from deeper sources. The sharp contacts between granitic outcrops with metavolcanics on the eastern and northern parts of the geologic map are clearly obvious on the various magnetic maps. They also confirm the great agreement of the magnetic intensity with surface geological structures, which indicate the extensions of these faults in depth. As can be seen the biotite granite shows values of the magnetic intensity higher than those of the albite granite, which may be due to an increase content of magnetic minerals in biotite granite than that in albite granite.

The regional–residual separation of magnetic anomalies was applied to the RTP magnetic map of the study area. Two main average magnetic interfaces at depths of 0.6 and 1.7 km below the measuring level were calculated through the application of a power spectrum technique (Fig. 7). Filtering assisted in the discrimination between shallow and deep-seated sources of magnetic anomalies and produced the regional and residual magnetic-component maps (Figs. 8 and 9).

The high magnetic contrast along the contacts of acidic and basic rocks clearly reflects mostly sharp contacts, as shown on

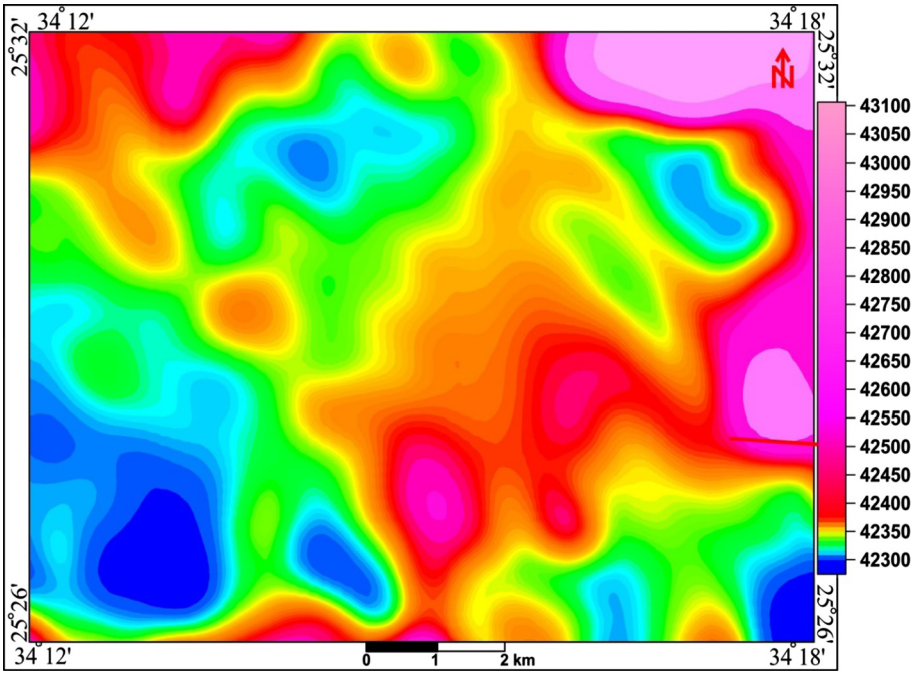

Fig. 6 Airborne magnetic field intensity image map, reduced to the north pole of Um Naggat area.

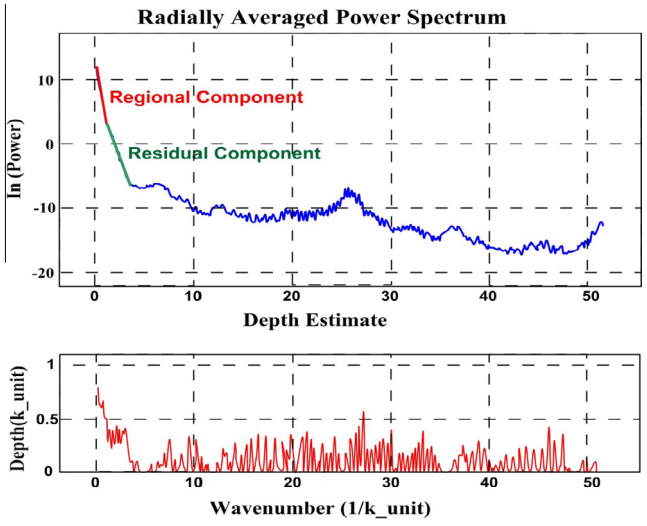

Fig. 7 Spectrum frequency for the airborne RTP magnetic field intensity data of Um Naggat area.

the regional magnetic-component map (Fig. 8). The elongated stretch of low magnetic values generally corresponds with granitic rocks. Meanwhile, the broad and high magnetic patterns seen at the eastern and northeastern parts of the study area represent generally metavolcanics. Since the magnetic intensities of biotite granite decrease gradually towards the southwest, therefore, the lowest magnetic values in the study area may reflect the source of granitic magma, i.e., from the southwest direction. The oval-shaped low magnetic anomaly that is associated with albite granite indicates that it is deep-seated, that resulted from highly-differentiated patch of albite granite. The residual magnetic map (Fig. 9) helped to attenuate broad, more regional anomalies and enhance local, more subtle magnetic responses, because of their sensitivity to shallow magnetic source bodies and contacts. It also helped to draw and deduce the subtle extensions of various structures enhanced by other filtered grids. The residual magnetic component image map (Fig. 9) indicates that Um Naggat geological units were fractured and faulted by different tectonic regimes. The granitic pluton is more tectonically disturbed, increasing rock permeability, and thus, had the potential to host hydrothermal fluids. Some faults were not clearly noticed on the regional component magnetic map (Fig. 8), but were well exposed on the residual one (Fig. 9). Three high anomalous zones, trending in the NE–SW direction, which are associated with metavolcanics units, are observed on this image. Fig. 10 is a representation of the delineated magnetic structural lineaments superimposed on the RTP and residual magnetic maps (Figs. 6 and 9). This interpreted structural map gives an idea about the depositional time-sequence of formation of the lithological units and some geological structures in Um Naggat area. The interpreted magnetic structural map reveals enhanced structural features that include faults, shears, fault intersections and fracture systems that mainly trend NW-, NNW- and ENE-directions. This is quite obvious where there are a large number of magnetic markers striking perpendicular to these structures. The most important and perhaps the youngest trends of these structures extend in the NW- and NNW-directions because it is characterized by a long length of extension and cutting most of the rock units of the studied area. The oldest phase of the structural lineaments or faults extends in the ENE-direction that dissects and displaces, with right lateral movement from the youngest structures.

4.3. Geochemical data

The results of geochemical and mineralogical analyses are summarized in Table 1. Um Naggat albite granites represent

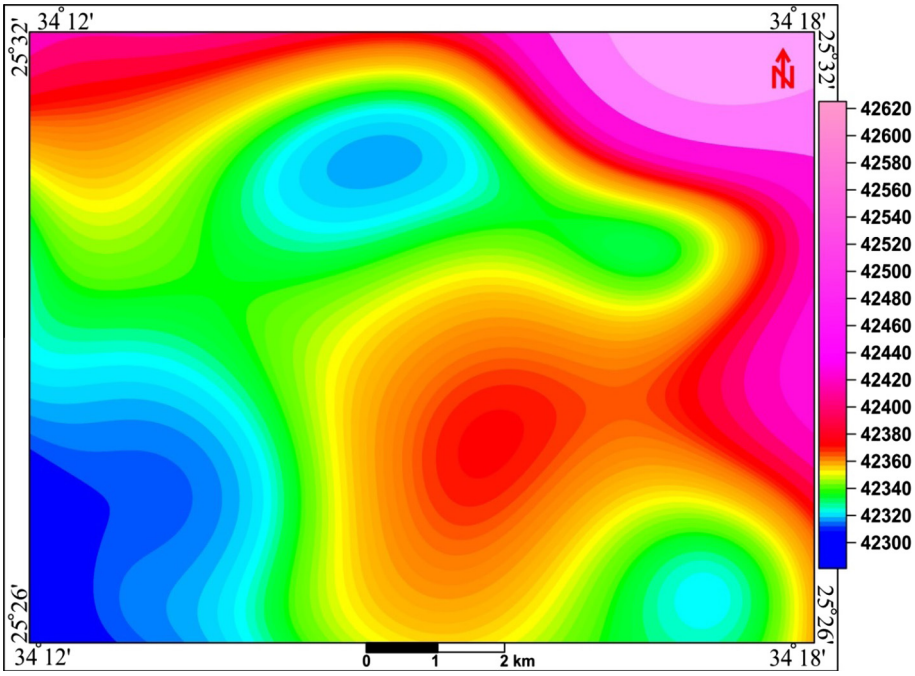

Fig. 8 Airborne regional-component magnetic field intensity image map of Um Naggat area.

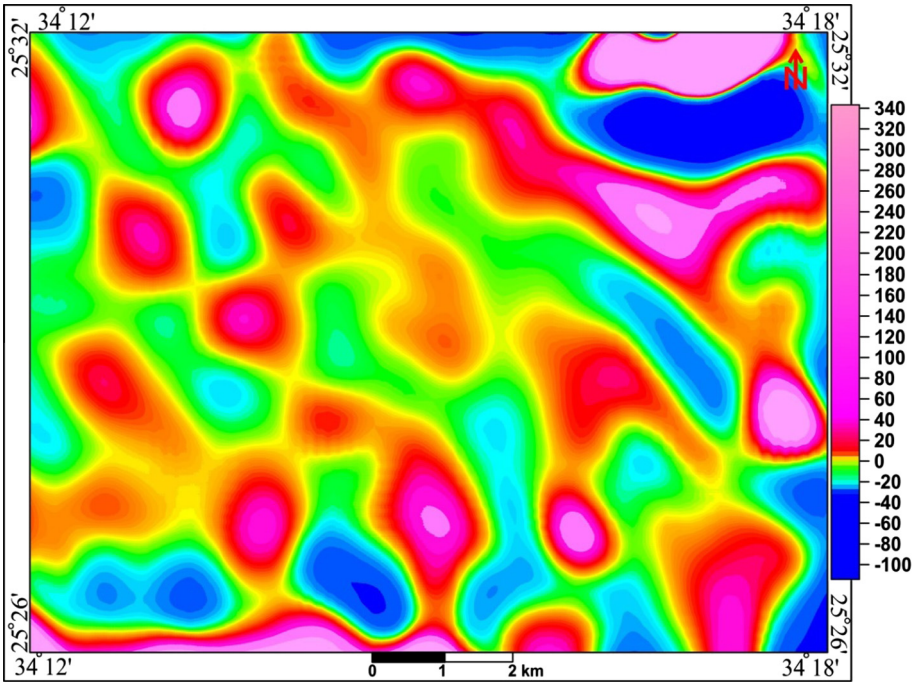

Fig. 9 Airborne residual-component magnetic field intensity image map of Um Naggat area.

a case of extreme metal enrichment (U, Th, REE, Zr) from associated granitic melts, with limited fluid/melt migration. This enrichment occurred at very high temperatures and very high fluorine activities. This allowed the migration of very low soluble elements (Th, Zr and REE) together with U. They may derive a part or all of their enrichment from such processes and not only from partial melting of an U–Th–REE-rich protolith as is usually proposed (Cuney and Kyser, 2008; Mercadier et al., 2013).

The potential of U mineralization in granite is governed by many factors, not only the U content of granitic magma but also the physical–chemical conditions. The abundance of (F) has a great role in decreasing crystallization temperature, degree of oxidation, and concentration of U in granitic magma

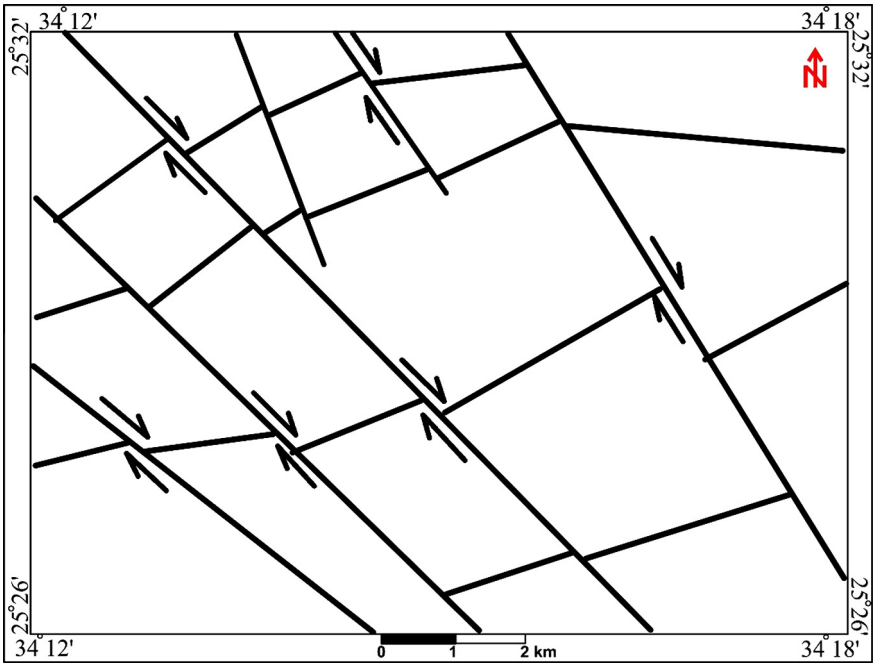

Fig. 10 Structural lineaments map as deduced from the aeromagnetic data of Um Naggat area.

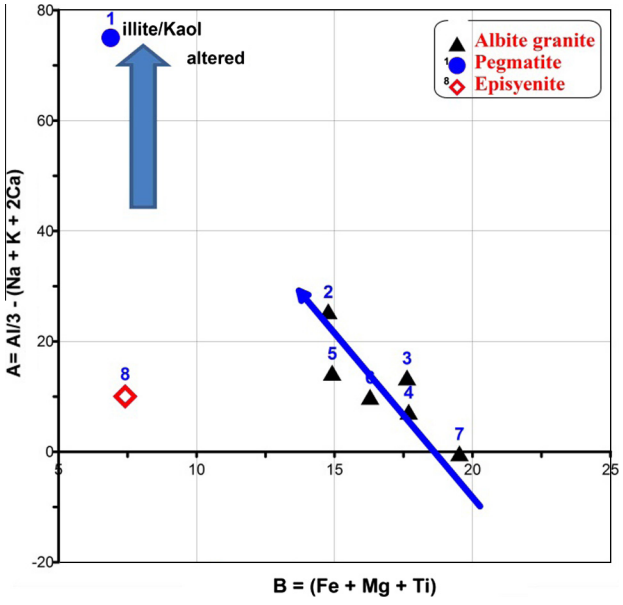

Fig. 11 Variation of the peraluminous index (A) with fractionation index (B), for Um Naggat area. A–B mineralogical–chemical diagram, from Debon and Lefort (1988).

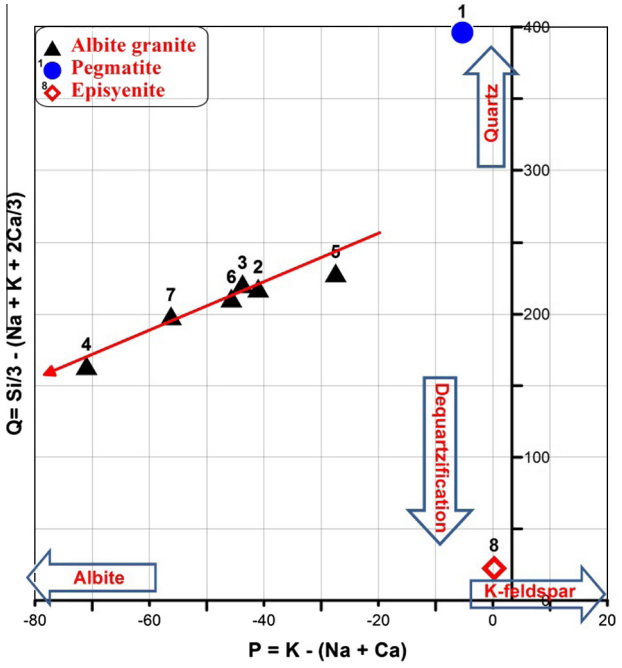

Fig. 12 Variation of the K-feldspar/albite (P parameter) versus quartz contents (Q parameter) for Um Naggat area. Q–P mineralogical–chemical diagram from Debon and Lefort (1988).

(Zhao et al., 2011; Chen et al., 2012). A foregoing study demonstrated that uranium oxides have REE abundances directly dependent on the geological conditions linked to uranium oxide formation and are a key for defining meaningful genetic models (Mercadier et al., 2011).

4.3.1. Major element concentrations

The major element oxide contents of granites in the studied areas are given in Table 1. The data show some differences and similarities between these granites. The albite granites of Um Naggat have the highest contents of SiO_2 (75–78%). The episyenite samples of Um Naggat have the highest contents of K_2O (8.1%), Na_2O (5.3%), Al_2O_3 (18.2%) but the lowest ones of SiO_2 (66.1%). Albite granites have the highest content of Fe_2O_3 (1.2–1.5%) whereas the episyenite and pegmatite samples show the lowest Fe_2O_3 (0.6%) content.

Fig. 11 of the relationship between A and B shows an inverse relationship for each of Um Naggat samples and confirms that all samples of the studied area are located within the peraluminous field. This inverse relationship was drawn by an arrow representing the general trend for all the samples. It is noted that the pegmatite and episyenite samples from Um Naggat area are located in the alteration fields, separately from the rest of the samples.

The relationship between Q and P (Fig. 12) shows a direct relationship for most of the samples of the studied area. It is noticed that the northern margin of Um Naggat pluton tends to increase in albite. The sample (No. 8) of Um Naggat area shows depletion of its silicate content that confirms that it is episyenite. The pegmatite sample (No. 1) shows silicification, i.e., enrichment in SiO_2 and therefore, lies in the quartz field.

4.3.2. Trace element distributions

Van Lichtervelde et al. (2010) and Linnen et al. (2012) showed that U-, Th-, Nb-, Y- and REE-minerals are closely linked to highly-fluxed silicate melts. Fluxes, including F and P, are important for the transport and deposition of these metals, depending on their melt composition.

The Rb–Sr relation for Um Naggat area develops in one evolution trend where Sr decreases and Rb increases towards magma evolution (Fig. 13). An increase in Rb/Sr values from the core to the periphery of albite granite was documented (Fig. 13). Rb is incorporated in K minerals and Sr in Ca minerals and hence, the Rb/Sr ratio amplifies any increase in K or loss in Ca in hydrothermal alteration zones. Granites associated with mineralization commonly have a high Rb/Sr ratio, as a result of fractionation. It is concluded that the ratios may be useful as a guide to different types of mineralization in albite granite.

Radioactive potentiality as shown in airborne γ-ray spectrometric surveys revealed that the albite granite exhibits high uranium anomalies (up to 90 ppm eU), as compared to the biotite granite (2–12 ppm eU). The plot of U versus Th content of Um Naggat facies shows a fairly positive correlation and gross enrichment from the lower alkali feldspar granite zone to the albite and pegmatite zone (Fig. 14). Fresh albite granite shows enhanced contents of both elements (U & Th)', with average Th/U ratio of about 2.0, which is lower than the values of igneous system (3.5–4.0) (Rogers and Adams, 1969). However, during the process of albitization there is a pronounced enrichment in U (av. 50 ppm) and to a lesser extent

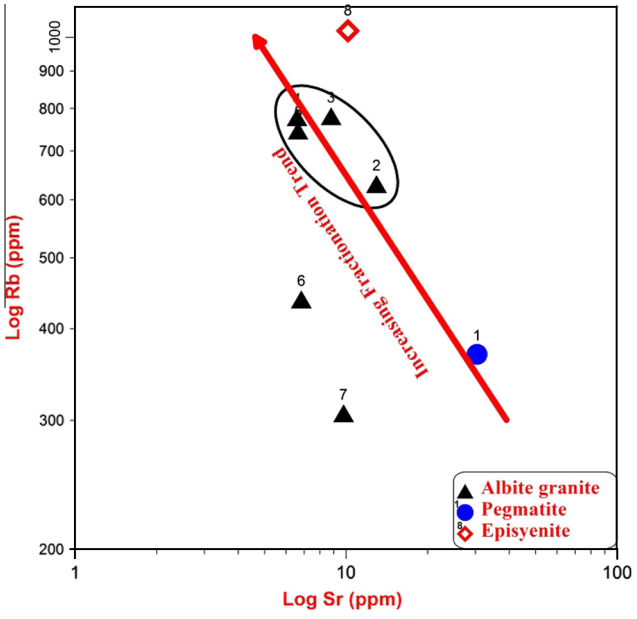

Fig. 13 Rb–Sr relation reflects an increase in Rb/Sr values from the core to the periphery of albite granite, Um Naggat area.

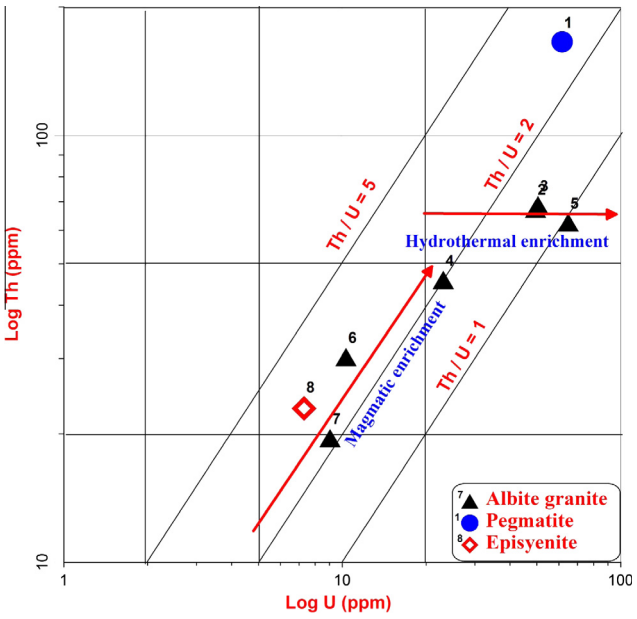

Fig. 14 Th versus U variation diagram in Um Naggat granites indicates that U is enriched during fractionation, Um Naggat area.

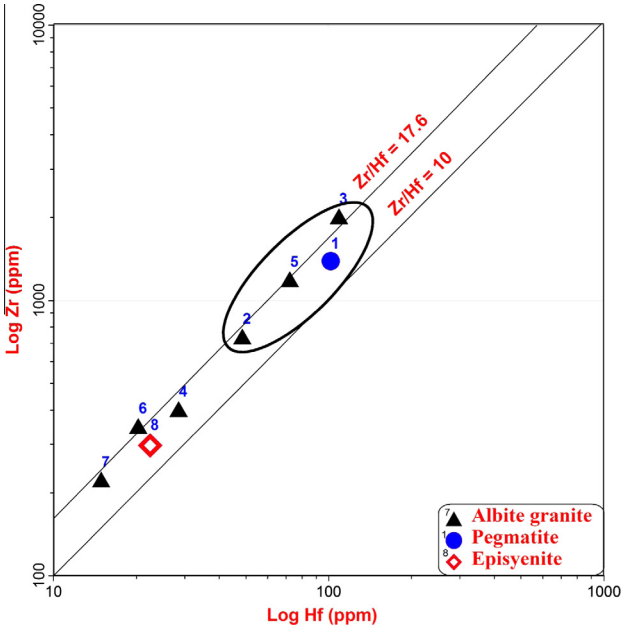

Fig. 15 Zr–Hf binary relation in the different facies of Um Naggat area shows a good positive correlation with more or less fixed ratios of Zr/Hf = 15, Um Naggat area.

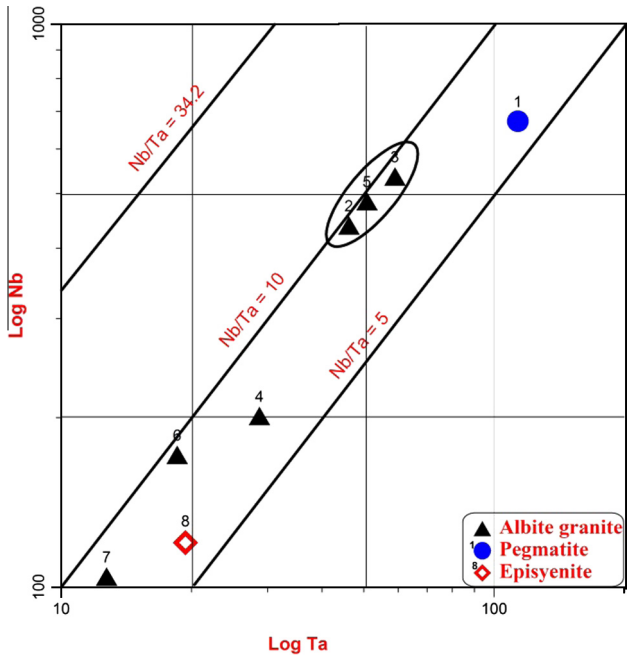

Fig. 16 Nb–Ta binary relation in the different facies of Um Naggat area shows a good positive correlation with increasing of both Nb and Ta towards the periphery, Um Naggat area.

in Th (av. 60 ppm). Meanwhile, the Th/U ratio (av. 1.1) becomes less than that of the unaltered albite granite. Lowering of the Th/U ratio and its deviation from the coherent values of albite granite at the northern periphery, generally indicate redistribution of uranium and possible evidence for uranium accumulation.

The relationship between hafnium- and zirconium shows a positive relationship with an increase towards the northern part of albite granite (Fig. 15). Um Naggat area has a wide range for both hafnium and zircon, which lies in the moderate level with Zr/Hf ratio of about 15. This ratio shows a slight increase of hafnium relative to zircon where the normal ratio is 17.6. Fig. 16 shows that the samples of Um Naggat area are aligned around the ratio of Nb/Ta = 9 with niobium values ranging from 100 to 1000 ppm and its coherent tantalum content ranges between 10 and 100 ppm, whereas the normal ratio of Nb/Ta is 34.2. This indicates the increase of niobium compared to tantalum, with increasing fractionation.

The Nb–Ta and Zr–Hf pairs exhibit an inherited fractionation level of evolved albite granite, which was preserved during the course of extraction and transportation by post-magmatic fluids. The inherited predominance of Nb over Ta and Zr over Hf in the albite granite can be attributed to igneous fractionation, characterizing Um Naggat area. The well-defined fractionation trends in both columbite and zircon minerals are mostly associated with albite and pegmatite. The concurrent enrichment of both zircon and HREE in the albitized granite indicates that this mineral controls the HREE abundance during Na-metasomatism.

The concurrent enrichment of U, Nb, Ta and Zr in albite granite and pegmatite may indicate that U can be partly incorporated within zircon and columbite. The greater the mineralogical sites of U and the accompanying rare metals, the greater the potential significance of U-bearing fluids. The estimated reserves of Zr and Nb in Um Naggat albite granite are 75,000 and 45,000 tons, respectively (Zalata et al., 1972).

Although Um Naggat granite has much alteration processes such as albitization, greisenization, kaolinization and fluoritization at the northern part of the granitic body as well as many silica injections, it has a degree of low fractionation to represent a source for further hydrothermal or supergene U-concentration except the northern part of albite granite. Therefore, this granitic pluton is considered as a low U-favourability, except its periphery of albite granite. The northern part of Um Naggat granite presents an example of a limited U-enrichment in the albitized rim (up to 200 ppm), but U being mainly bound to refractory mineral phases; thus, it is highly improbable to discover richer facies at depth. The highly differentiated phase, and the low unexpected U-favourability for this phase are due to thorium and rare earth elements (REE) that were soluble in the silicate melts, so they are not fractionated in early crystallization of accessory minerals. Consequently, during magmatic differentiation uranium is enriched simultaneously with Th, REE and other incompatible elements. Thus, this phase will be rich in Th, REE and U, but uranium is strongly held in the structures of refractory minerals. So, it is not easily leachable by hydrothermal solutions especially if they are formed closely after magma emplacement and crystallization (Cuney and Friedrich, 1987).

5. Conclusions

The present work aimed to identify and delineate mineralized zones in Um Naggat area by integrating the geological, geophysical and mineral chemistry data. The reconstructed geological map with radiometric and magnetic data sets, established links between lithology, structures and hydrothermal alteration patterns and identified albite granite bearing Nb–Ta-, Zr–Hf, REE, Th–U. The radiometric data are an excellent tool for mapping and tracing individual lithological units in areas of outcrop. The mafics and ultramafics units are distinctive in K, eU, eTh and RBG maps, because of their low radiometric signatures. The albite granites have a high total count radiometric response, appearing as white or blue colours (high uranium) in the ternary image. Such domains host the known rare-metal mineralization, illustrating the utility of -ray spectrometric data to improve geologic maps. The principal geological structures hosting many of the rare metal deposits include faults, fractures and shear zones that play the most important role in Nb, Ta, U mineralization in the Um Naggat area. The continuous reactivations of these structures have a profound effect on both the distribution and mode of mineralization. Therefore, the delineated structures of the study area are likely to be potential hosts of metal ore mineralization. Interpretations of the reconstructed aeromagnetic maps delineated four regional structural trends oriented towards NNW-, NW-, ENE- and E–W directions identified as strike-slip faults, which coincide with field observations where the NW-directions faults cut and displace right laterally the ENE–WSW older ones. The interaction between these two strike-slip fault systems configuring the albite granite, is easily identified in the regional data presenting the longer wavelength anomalies implying deep-seated structures that could be the potential pathways for the enriched mineralized fluid migration.

These regions also recorded high U and Th, but low K concentration, thus, qualified for hydrothermally-altered zones. High structural connectivity in the albite granite of intensive alterations, reflected as low magnetic and high radiometric anomalies. The hydrothermal alteration zone that is associated with albite granite can also be considered as structurally controlled. Moreover, the area is also marked by huge alteration in concordant with the albite granite, indicating a region of higher fluid pressure and accumulation.

Um Naggat albite granite confirms that all gathered samples are located in the peraluminous field. Episyenite is located in alteration field due to depletion of their silicate content whereas pegmatite shows silicification. The high level of rare-metal mineralization in the periphery of albite granite compared to core shows possibly a high influence of metasomatism in the mineralization process. They are clearly enriched in niobium compared to tantalum and the trend of enrichment as clearly Nb $\gg$ Ta. Trace element data show appreciable content of rare metals in all samples. The pegmatite sample contains much higher Nb with average content of 672 ppm. This sample has the highest Ta mean values of 113 ppm, while the lowest Ta values are recorded for the episyenite and albite granite near the core (12.7–19.4 ppm). All rock samples are enriched in Rb (307–1021 ppm) and depleted in Sr (6.6–30 ppm). The ratios Nb/Ta (7–10) and Zr/Hf (14–18) are relatively enriched in the lighter isovalents Ta and Hf whereas the normal ratios are 34.2 and 17.6 respectively. The Rb/Sr ratio shows variability in all the samples with an average of 90 ppm. The Nb/Ta ratio clearly shows that the Nb is preferred relative to Ta. Within all the samples the highest ratio of about 10 is related to the periphery albite samples compared with about 7 in the whole rock samples. An increase in Rb/Sr values from the core to the periphery of the albite granite has been documented as a result of fractionation and consequently associated with mineralization. Um Naggat granitic pluton is however considered as a low U-favourability, except, its northern part of albite granite. Lowering of the Th/U ratio in the periphery (albite granite) indicates redistribution of uranium and possible evidence for uranium accumulation at depth.

References

Aero Service, 1984. Final operational report of airborne magnetic/radiation survey in the Eastern Desert, Egypt. Aero-Service Division, Houston, Texas, USA, Six Volumes.

Airo, M.-L., Loukola-Ruskeeniemi, K., 2004. Characterization of sulfide deposits by airborne magnetic and gamma ray responses in eastern Finland. Ore Geol. Rev. 24, 67–84.

Chaturvedi, A.K., Lotter, C., Tripathi, S., Maurya, A.K., Patra, I., Parihar, P.S., 2013. Integrated application of heliborne and ground electromagnetic surveys for mapping EM conductor for uranium exploration and its subsurface validation, North Delhi Fold Belt, Rajasthan, India: a case study. Geophysics 78 (1), B13–B24.

Chen, Y.-W., Bi, X.-W., Hu, R.-Z., Dong, S.-H., 2012. Element geochemistry, mineralogy, geochronology and zircon Hf isotope of the Luxi and Xianzhuang granites in Guandong Province, China: implications for U mineralization. Lithos 150, 119–134.

Cuney, M., Friedrich, M., 1987. Physicochemical and crystal-chemical controls on accessory mineral paragenesis in granitoids: implications for uranium metallogenesis. Soc. Francaise Mineral. Cristall., Paris 110, 235–247.

Cuney, M., Kyser, T.K., 2008. Deposits related to partial melting. In: Cuney, M., Kyser, T.K. (Eds.), . In: Recent and Not-so-recent Developments in Uranium Deposits and Implications for Exploration, Short Course Series, vol. 39. Mineralogical Association of Canada, Québec, pp. 79–95.

Debon, F., Lefort, P., 1988. Cationic classification of common plutonic rocks and their magmatic associations: principles, methods, applications. Bull. Minéral. 111, 493–510.

Direen, N.G., Lyons, P., Korsch, Glen R.A., 2001. Integrated geophysical appraisal of crustal architecture in the eastern Lachlan Orogen. Explor. Geophys. 32, 252–262.

El-Gaby, S., List, F.K., Tehrani, R., 1988. Geology evolution and metallogenesis of the Pan African belt in Egypt. In: El-Gaby, S., Greiling, R.O. (Eds.), The Pan African Belt of Northeast Africa and Adjacent Areas. Braun-Schweig (Vieweg), pp. 17–68.

Gaafar, I.M., 2012. Geophysical signature of the vein-type uranium mineralization of Wadi Eishimbai, Southern Eastern Desert, Egypt. Arab. J. Geosci. 5, 1185–1197.

Gaafar, I.M., 2014. Geophysical mapping, geochemical evidence and mineralogy for Nuweibi rare metal albite granite, Eastern Desert, Egypt. Open J. Geol. 4, 108–136.

Greiling, R.O., Kröner, A., El Ramly, M.F., Rashwan, A.A., 1988. Structural relationships between the southern and central parts of the Eastern Desert of Egypt: details of a fold and thrust belt. In: El-Gaby, S., Greiling, R.O. (Eds.), The Pan-African Belt of Northeast Africa and Adjacent Areas. Vieweg Publisher, Wiesbaden-Braunschweig, Germany, pp. 121–146.

Irvine, R.J., Smith, M.J., 1990. Geophysical exploration for Epitermal deposits. J. Geochem. Explor. 36, 375–412.

Linnen, R.L., Van Lichtervelde, M., Černý, P., 2012. Granitic pegmatites as sources of strategic metals. Elements 8, 275–280.

Manu, J., 1993. Gold deposits of Birimian greenstone belts in Ghana: hydrothermal alteration and thermodynamics. Verlag Mainz, Wissenchaftsverlag, Aachen Herstellung: Fotodruck Mainz GmbH Susterfeldstr. vol. 83, Aachen. pp. 52–72.

Mercadier, J., Cuney, M., Lach, P., Boiron, M., Bonhoure, J., Richard, A., Leisen, M., Kister, P., 2011. Origin of uranium deposits revealed by their rare earth element signature. Terra Nova, 1–6.

Mercadier, J., Annesley, I.R., Mc Kechnie, C.L., Bogdan, T.S., Creighton, S., 2013. Magmatic and metamorphic uraninite mineralization in the western margin of the Trans-Hudson Orogen (Saskatchewan, Canada): a uranium source forum conformity-related uranium deposits? Econ. Geol. 108, 1037–1065.

Mohanty, W.K., Mandal, A., Sharma, S.P., Gupta, S., Misra, S., 2011. Integrated geological and geophysical studies for delineation of chromite deposits: a case study from Tangarparha, Orissa, India. Geophysics 76, B173–B185.

Moreira, C.A., Ilha, L.M., 2011. Prospecção geofísica em ocorrência de cobre localizadana bacia sedimentar do Camaquã (RS). Revista da Escola de Minas, Ouro Preto 64 (3), 309–315.

Moreira, C.A., Lopes, S.M., Schweig, C., Seixas, A.R., 2012. Geoelectrical prospection of disseminated sulfide mineral occurrences in Camaquã sedimentary basin, Rio Grande Sul State, Brazil. Revista Brasileira de Geofísica 30 (2), 169–179.

Murphy, B.S., 2007. Airborne geophysics and the Indian scenario. J. Ind. Geophys. Union 11 (1), 1–28.

Patra, I., Chaturvedi, A.K., Srivastava, P.K., Ramayya, M.S., 2013. Integrated interpretation of satellite imagery, aeromagnetic, aeroradiometric and ground exploration data sets to delineate favorable target zones for unconformity related uranium mineralization, Khariar Basin, Central India. J. Geol. Soc. India 81, 299–308.

Rogers, J.J.W., Adams, J.A., 1969. Uranium in geochemistry. In: Wedepohl, K.H., (Ed.), 4, B2, Springer Verlag, Berlin.

Sabet, A.H., Zhukov, M.A., Babourin, L.M., Mansour, M.G., 1976. Rare metal apogranites in Um Naggat massif. Egypt. Geol. Surv., Ann. 6, 191–200.

Schetselaar, E.M., 2001. Petrogenetic interpretation from gamma-ray spectrometry and geological data: the Arch Lake zoned peraluminous granite intrusion. Western Canadian Shield. Explor. Geophys. 33, 35–43.

Shives, 2008. Spectrometric data related to Mammaslhti Cu–Zn–Au deposit in eastern Finland. Special paper 31, pp. 97–103.

Silva, A.M., Pires, A.C., Mc Cafferty, A., Moraes, R., Xia, H., 2003. Application of airborne geophysical data to mineral exploration in the uneven exposed terrains of the Rio Das Velhas greenstone belt. Revista Brasileira de Geociências 33 (2), 17–28.

Stern, R.J., 1981. Petrogenesis and tectonic setting of Late Precambrian ensimatic rocks. Central E.D., Egypt. Precambrian Res. 16, 195–230.

Telford, W.M., Geldart, L.P., Sheriff, R.E., 1990. Applied Geophysics, second ed. Cambridge University Press.

Van Lichtervelde, M., Holtz, F., Hanchar, J.M., 2010. Solubility of manganotantalite, zircon and hafnium in highly fluxed peralkaline to peraluminous pegmatitic melts. Contrib. Mineral Petrol 160, 17–32.

White, A.F., Bullen, T.D., Schulz, M.S., Blum, A.E., Huntington, T.G., Peters, N.E., 2001. Differential rates of feldspar weathering in granitic regoliths. Geochim. Cosmochim. Acta 65, 847–869.

Zalata, A.A., et al., 1972. Reports on the results of prospecting work for gold and rare metals by the Barramiya party in the area of Barramiya in 1971–1972. Internal Rept., Egypt. Geol. Suiv., Cairo. (Editorial handling 1 Hidehiko Shimazaki).

Zhao, K.-D., Jiang, S.-Y., Dong, C.-Y., Chen, W.-F., Chen, P.-R., Ling, H.-F., Zhang, J., Wang, K.-X., 2011. Uranium-bearing and barren granites from the Taoshan Complex, Jiangxi Province, South China: geochemical and petrogenetic discrimination and exploration significance. J. Geochem. Explor. 110, 126–135.